Canonical Space–Time Processing for Wireless Communications

Eko N. Onggosanusi, Akbar M. Sayeed, *Member, IEEE*, and Barry D. Van Veen, *Senior Member, IEEE*

***Abstract*—A canonical space–time characterization of mobile wireless channels is introduced in terms of a fixed basis that is independent of the true channel parameters. The basis captures the essential degrees of freedom in the received signal using discrete multipath delays, Doppler shifts, and directions of arrival (DOA). The canonical representation provides a robust representation of the propagation dynamics and eliminates the need for estimating delay, Doppler and DOA parameters of different multipaths. Furthermore, it furnishes a natural framework for designing low-complexity space–time receivers. Single-user receivers based on the canonical channel representation are developed and analyzed. It is demonstrated that the resulting canonical space–time receivers deliver near-optimal performance at substantially reduced complexity compared to existing designs.**

***Index Terms*—Antenna arrays, diversity methods, multipath, RAKE receiver, time-varying channels.**

I. Introduction

THE USE of antenna arrays for enhancing the capacity and quality of wireless communication systems has spurred significant interest in space–time signal processing techniques [1]. A key consideration in space–time receiver design is modeling the complex time-varying multipath propagation environment. Most existing receiver designs employ "ideal" matched filtering to all the dominant multipaths and corresponding direction of arrivals (DOAs). In addition to suffering from high computational complexity in a dense multipath environment, such receivers rely heavily on accurate estimation of the delay and DOA parameters of dominant scatterers [1]. It can be difficult to estimate these parameters in low SNR scenarios. The time-varying nature of the spatio-temporal channel requires continuous tracking of delay and DOA parameters which further complicates receiver design. The complexity of front-end processing can adversely affect other aspects of receiver design as well, including interference suppression, timing acquisition, and channel estimation.

In this paper, we introduce a canonical representation of the received signal in terms of a *fixed* finite-dimensional basis. The basis captures the essential degrees of freedom in the channel that are observable at the receiver and corresponds to certain discrete multipath delays, Doppler shifts, and DOAs of the signaling waveform. The canonical representation provides a robust representation of the propagation dynamics and eliminates the need for estimating delays, Doppler shifts, and DOAs of different multipaths. In essence, it is a parsimonious fixed representation of the signal with virtually no loss of information. In this paper, we focus on single-user code-division-multiple-access (CDMA) systems to illustrate the advantages of the canonical representation. We develop both coherent and noncoherent space–time receiver structures. It is demonstrated that the canonical receiver structures deliver near-optimal performance at a dramatically reduced complexity compared to existing designs, especially in dense multipath environment.

There have been several recent works that exploit the use of fixed basis signals for modeling and estimating the wireless channel (see, e.g., [2]–[4]). All these works focus on temporal processing and slow fading environment. This paper develops a model for an arbitrary spatio-temporal channel and fully incorporate fast fading effects along the lines of [5]. We note that temporal channel variations are also modeled via basis signals in [6]. However, in contrast to the fixed basis philosophy of this paper, the basis signals used in [6] depend on channel parameters such as Doppler frequencies.

The canonical channel representation is developed in the next section. Single-user coherent and noncoherent receiver designs are discussed in Section III. The performance of the receivers is analyzed in Section IV. Section V demonstrates the advantages of canonical space–time receivers via various examples. Conclusions and avenues for future research are discussed in Section VI.

II. Canonical Space–Time Signal Representation

The received complex baseband signal vector $\mathbf{r}(t)$ at an R-element sensor array due to a single symbol from a single user is

$$\mathbf{r}(t) = \mathbf{s}(t) + \mathbf{n}(t) \tag{1}$$

where $\mathbf{s}(t)$ and $\mathbf{n}(t)$ are the R-dimensional information bearing signal and complex white Gaussian noise, respectively. The signal component at the kth element in the array is

$$s_k(t) = \int_{S^-}^{S^+} e^{-j2\pi \frac{c}{\lambda}\tau_k(\phi)} x(\phi, t)\, d\phi, \qquad k = 1, 2, \ldots, R$$

where $x(\phi, t)$ denotes the signal waveform arriving from direction ϕ, λ denotes the carrier wavelength, and c denotes the speed of propagation. As illustrated in Fig. 1, $[S^-, S^+]$ is the angular

Paper approved by B. L. Hughes, the Editor for Theory and Systems of the IEEE Communications Society. Manuscript received June 30, 1999; revised January 7, 2000. This paper was presented in part at the IEEE International Conference on Acoustics, Speech, and Signal Processing, Phoenix, AZ, March 1999.

The authors are with the Department of Electrical and Computer Engineering, University of Wisconsin–Madison. Madison, WI 53706 USA (e-mail: vanveen@engr.wisc.edu).

Publisher Item Identifier S 0090-6778(00)08774-2.

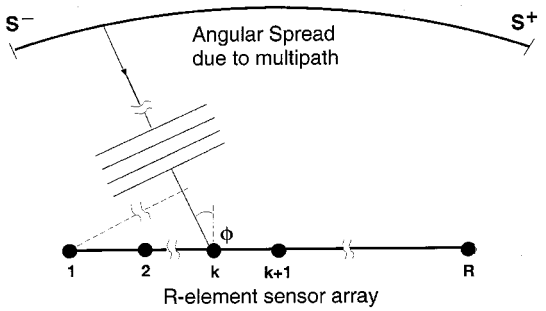

Fig. 1. Signal reception geometry.

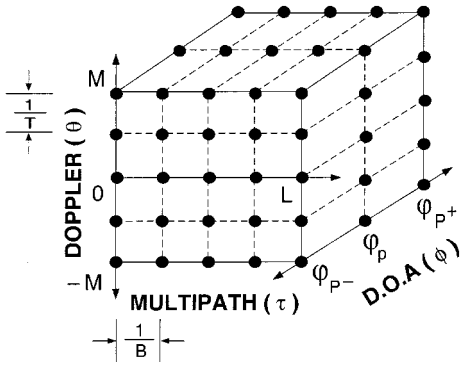

Fig. 2. A schematic depicting the canonical space–time coordinates.

spread of the scatterers encountered during propagation,[1] and $\tau_k(\phi)$ is the time delay of the signal waveform at the kth antenna element relative to the first antenna element. The received signal $x(\phi,t)$ is related to the transmitted signaling waveform $q(t)$ of duration T via the angle-dependent time-varying channel impulse response $h(\phi,t,\tau)$ or, equivalently, the multipath-Doppler spreading function $H(\phi,\theta,\tau)$ [7], [8]

$$x(\phi,t) = \int_0^{T_m} h(\phi,t,\tau)q(t-\tau)\,d\tau = \int_0^{T_m}\int_{-B_d}^{B_d} H(\phi,\theta,\tau)q(t-\tau)e^{j2\pi\theta t}\,d\theta\,d\tau \quad (2)$$

where T_m and B_d denote the multipath and Doppler spreads, respectively.[2] Without loss of generality, we choose $q(t)$ to have unit energy with support $[0,T)$. Defining the array response vector as a function of ϕ as

$$\mathbf{a}(\phi) = \left[1, e^{-j2\pi\frac{c}{\lambda}\tau_2(\phi)}, \ldots, e^{-j2\pi\frac{c}{\lambda}\tau_R(\phi)}\right]^T \Big/ \sqrt{R} \quad (3)$$

we can express the received signal in a vector form as follows:

$$\mathbf{s}(t) = \int_{S^-}^{S^+} \mathbf{a}(\phi)x(\phi,t)\,d\phi. \quad (4)$$

A discretized version of (2) is often used for system design and analysis

$$\mathbf{s}(t) = \sum_{l=1}^{L_T} \beta_l \mathbf{a}(\phi_l)e^{j2\pi\theta_l t}q(t-\tau_l) \quad (5)$$

where L_T is the number of (dominant) scatterers, $\beta_l(t)$ is the time-varying complex path fading coefficient, and $\phi_l \in [S^-,S^+]$ and $\tau_l \in [0,T_m]$ are the DOA and path delay corresponding to the lth path.

A. Canonical Signal Representation

The signal experiences temporal and spatial dispersion during propagation as evident from (2). Our characterization of the information bearing signal is motivated by the fact that the signaling waveform $q(t)$ has a finite duration T and an essentially finite bandwidth B. Hence, the signal $x(\phi,t)$ exhibits only a finite number of *temporal* degrees of freedom that are captured by a set of uniformly spaced discrete multipath delays and Doppler shifts [5], [9][3]. Furthermore, assuming the antennas are spaced to avoid spatial aliasing, $\mathbf{s}(t)$ possesses at most R *spatial* degrees of freedom that can be captured by certain discrete DOAs even if the DOA distribution is continuous within $[S^-,S^+]$. The following canonical space–time characterization of $\mathbf{s}(t)$ identifies these essential spatio-temporal degrees of freedom in the channel that are *observable* at the receiver.

Theorem: The signal $\mathbf{s}(t)$ in (4) admits the canonical representation

$$\mathbf{s}(t) \approx \hat{\mathbf{s}}(t) = \sum_{p=P^-}^{P^+}\sum_{m=-M}^{M}\sum_{l=0}^{L} H_{pml}\mathbf{q}_{pml}(t), \qquad 0 \le t < T \quad (6)$$

in terms of the unit-energy space–time basis waveforms

$$\mathbf{q}_{pml}(t) = \mathbf{a}(\varphi_p)e^{j((2\pi mt)/T)}q\left(t-\frac{l}{B}\right) \quad (7)$$

where[4] $\{\varphi_1,\varphi_2,\ldots,\varphi_R\}$ are chosen such that $\{\mathbf{a}(\varphi_1),\ldots,\mathbf{a}(\varphi_R)\}$ are linearly independent and $-(\pi/2) \le \varphi_1 < \varphi_2 < \cdots < \varphi_R \le (\pi/2)$. The number of terms in (6) are given by $L = \lceil T_m B\rceil, M = \lceil TB_d\rceil, P^+ = \min_i\{\varphi_i : \varphi_i \ge S^+\}$, $P^- = \max_i\{\varphi_i : \varphi_i \le S^-\}$. □

The proof of this canonical representation is given in Appendix A. An alternate proof based on the finiteness of the array aperture is given in [11]. Fig. 2 illustrates the canonical space–time channel coordinates defined by the multipath-Doppler-angle sampling in the above representation. We note that the number of terms in the canonical coordinate expansion given above is the *minimum* to obtain a reasonably accurate representation of $\mathbf{s}(t)$ for an arbitrary channel. The main source of error is due to the band-limited approximation to the signaling waveform $q(t)$. It is shown in the next section that the representation accuracy can be improved arbitrarily by increasing both the number of terms in the expansion (6) and through the choice of B. We also note that for uniform linear array geometries with the time delay at the pth element relative to the first is given by $\tau_p(\phi) = (p-1)\,d\sin(\phi)/c$, where

[1]For simplicity of presentation we have assumed a one dimensional array.

[2]We note that T_m and B_d denote the maximum spreads—the variation of spreads with ϕ is captured by $H(\phi,\theta,\tau)$.

[3]This is related to Shannon's celebrated $2WT$ theorem (see, for example, [10]).

[4]Note that φ is used for canonical DOAs instead of ϕ to differentiate canonical spatial sampling from natural DOAs represented by ϕ.

d is the spacing between adjacent elements. If, furthermore, $d = \lambda/2$, then a set of orthogonal spatial basis vectors $\{\mathbf{a}(\varphi_p)\}$ can be obtained by choosing

$$\sin(\varphi_p) = \frac{2p - R - 1}{R}, \qquad p = 1, 2, \ldots, R. \tag{8}$$

While the canonical representation (6) is quite general, it proves particularly advantageous in the context of spread-spectrum ($TB \gg 1$) signaling [5]. From a signal representation viewpoint, it provides a robust and *parsimonious* characterization of space–time propagation effects in terms of the *fixed* basis given in (7). It is parsimonious in the sense that, amongst all fixed-basis representations, it yields the lowest-dimension signal representation that is valid for any spatio-temporal channel with given channel spreads. This is due to the fact that the maximum number of essential degrees of freedom induced by the temporal and spectral channel spreading is approximately $\lceil T_m B \rceil (2\lceil TB_d \rceil + 1) = (L+1)(2M+1)$ [5], [8], and the maximum number of degrees of freedom induced by spatial channel spreading is $\lceil (S^+ - S^-)/S_a \rceil \approx (P^+ - P^- + 1)$, where S_a denotes the sensor aperture [11]. These essential degrees of freedom are captured by a fixed basis in the canonical representation. Any fixed-basis signal representation will require at least $(L+1)(2M+1)(P^+ - P^- + 1)$ dimensions for characterizing all spatio-temporal channels with the given channel spreads. Consequently, the canonical representation also eliminates the need for estimating arbitrary delays, Doppler shifts, and DOAs of dominant scatterers.[5] Note that changes in the channel spread can be accomodated by simply adding or discarding some basis functions; the structure of the basis set does not change.

The representation also provides a versatile framework for channel modeling—both deterministic and stochastic. In particular, the $(P^+ - P^- + 1)(2M+1)(L+1)$ dimensional canonical channel coordinates defined by the basis (7) characterize the *inherent diversity level* afforded by a *wide-sense stationary uncorrelated scatterer* (WSSUS) channel [5], [9]. This is evident from (6) as the signal $\mathbf{s}(t)$ can be represented in terms of a finite number of the canonical basis waveforms. This indicates that the signal energy is located within a compact region of the canonical coordinate system.

Note that one may choose an "optimal" basis with a minimal number of nonzero expansion coefficients for a given signal $\mathbf{s}(t)$. However, such optimal bases are generally parameter-dependent. For example, an optimal set can be designed for given delays and DOAs of different paths. However, for a different set of delays and DOAs, all the basis signals in the set must be modified to preserve optimality. The representation (6) directly utilizes the *a priori* knowledge about the structure of the received signal—the array response $\mathbf{a}(\phi)$, the signaling waveform $q(t)$, and the channel spread parameters—to capture the essential degrees of freedom in the signal with respect to a *fixed* basis.

B. Computing Canonical Channel Parameters

The proof of the canonical signal representation in Appendix A is based on the time-limited and (essentially) band-limited nature of $q(t)$. In fact, the resulting channel parameters, which serve as the basis expansion coefficients in the representation, only depend on the duration T and bandwidth B of $q(t)$. However, the channel parameters derived in the proof are not necessarily optimal in any particular sense. A naturally optimal criterion to compute these channel parameters is to minimize the energy loss in reconstructing the signal $\mathbf{s}(t)$

$$\varepsilon_r = \int_{-\infty}^{\infty} \| \mathbf{s}(t) - \hat{\mathbf{s}}(t) \|_2^2 \, dt \tag{9}$$

where[6] $\| \mathbf{x} \|_2$ denotes the 2-norm of a vector $\mathbf{x}$. For analysis and derivation purposes, we define the vector space $\mathcal{C}^R \otimes \mathcal{L}_2$ for space–time signals of the form $\mathbf{s}(t)$ given in (4) with an inner product of two signals $\mathbf{x}(t)$ and $\mathbf{y}(t)$ defined as $\langle \mathbf{x}, \mathbf{y} \rangle_{\mathrm{ST}} \stackrel{\mathrm{def}}{=} \int \mathbf{y}^H(t)\mathbf{x}(t)\, dt$. Then, ε_r in (9) becomes $\| \mathbf{s} - \hat{\mathbf{s}} \|_{\mathrm{ST}}^2$, where $\| \mathbf{x} \|_{\mathrm{ST}}$ is the *space–time norm* of $\mathbf{x}$ induced by the inner product defined above. Note that $\| \mathbf{q}_{pml} \|_{\mathrm{ST}} = 1$.

In this section, we investigate the least squares optimal solution for the channel coefficients. We define the canonical array response matrix, temporal basis vector, and canonical channel parameter vector as follows:

$$\mathbf{A}_R = [\mathbf{a}(\varphi_{P^-}), \ldots, \mathbf{a}(\varphi_{P^+})] \tag{10}$$

$$\psi_R(t) = \left[e^{-j((2\pi M t)/T)}, \ldots, e^{j((2\pi M t)/T)} \right]^T \otimes \left[q(t), q\left(t - \frac{1}{B}\right), \ldots, q\left(t - \frac{L}{B}\right) \right]^T \Big/ \sqrt{T}$$

$$\hat{\mathbf{h}} = [\hat{H}_{P^-,-M,0}, \ldots, \hat{H}_{P^-,-M,L}, \ldots, \hat{H}_{P^-,M,0}, \ldots, \hat{H}_{P^-,M,L}, \hat{H}_{P^-+1,-M,0}, \ldots, \hat{H}_{P^-+1,-M,L}, \ldots, \hat{H}_{P^+,M,0}, \ldots, \hat{H}_{P^+,M,L}]^T$$

The symbol $\otimes$ denotes Kronecker product [12] and superscript T denotes matrix transposition. We may rewrite the canonical signal representation in (6) as

$$\hat{\mathbf{s}}(t) = \mathbf{U}_R \mathbf{Q}_R(t) \hat{\mathbf{h}} \tag{11}$$

$$\mathbf{U}_R \stackrel{\mathrm{def}}{=} \mathbf{A}_R \otimes \mathrm{ones}(1, (L+1)(2M+1))$$

$$\mathbf{Q}_R(t) \stackrel{\mathrm{def}}{=} \mathrm{diag}\{\psi_R(t)\} \otimes \mathbf{I}_{(P^+ - P^- + 1)}. \tag{12}$$

Here, ones (I, J) is an $I \times J$ matrix with unity for all entries, and $\mathrm{diag}\{\mathbf{v}\}$ forms a diagonal matrix from the elements of a vector $\mathbf{v}$. With this notation, it can be shown that the solution of the least squares problem (9) is

$$\hat{\mathbf{h}} = \arg\min_{\mathbf{h}} \| \mathbf{U}_R \mathbf{Q}_R(t)\mathbf{h} - \mathbf{s}(t) \|_{\mathrm{ST}}^2 = \mathbf{R}_w^{-1}\mathbf{d}$$

$$\mathbf{d} = \int_{-\infty}^{\infty} \mathbf{Q}_R^H(t)\mathbf{U}_R^H \mathbf{s}(t)\, dt,$$

$$\mathbf{R}_w \stackrel{\mathrm{def}}{=} \int_{-\infty}^{\infty} \mathbf{Q}_R^H(t)\mathbf{U}_R^H \mathbf{U}_R \mathbf{Q}_R(t)\, dt. \tag{13}$$

[5]Up to synchronization to a "global" delay, Doppler offset, and DOA to "align" the basis, which is required in all receivers.

[6]The integral is defined over the real line even though $\mathbf{s}(t)$ and $\hat{\mathbf{s}}(t)$ represent a single symbol. This accomodates an arbitrary multipath spread.

The resulting minimized reconstruction error is

$$\varepsilon_{r,\,\mathrm{MIN}} = \int \mathbf{s}^H(t)\mathbf{s}(t)\,dt - \mathbf{d}^H\mathbf{R}_w^{-1}\mathbf{d}. \tag{14}$$

The magnitude of $\varepsilon_{r,\,\mathrm{MIN}}$ depends on various parameters. However, we can decompose it into three parts, each corresponding to approximation in multipath, Doppler, and space domain. The error bound for general spatio-temporal time-varying channel is

$$\begin{aligned}\sqrt{\varepsilon_{r,\,\mathrm{MIN}}} \le\ & C_{\mathrm{angle}}\sqrt{\varepsilon_{r,\,\mathrm{angle}}} + C_{\mathrm{doppler}}\sqrt{\varepsilon_{r,\,\mathrm{doppler}}} \\ & + C_{\mathrm{mpath}}\sqrt{\varepsilon_{r,\,\mathrm{mpath}}}\end{aligned} \tag{15}$$

where $C_{\mathrm{angle}}, C_{\mathrm{doppler}}, C_{\mathrm{mpath}}$ are some constants. The first term $\varepsilon_{r,\,\mathrm{angle}}$ represents the reconstruction error in angle alone, which can be made arbitrarily small by the choice of array geometry and increasing the number of terms in the summation over p (see Appendix B). The second term $\varepsilon_{r,\,\mathrm{doppler}}$ represents the reconstruction error in Doppler only. The Doppler bases $e^{j2\pi mt/T}$ imply a Fourier series expansion for the Doppler spectrum, and hence, this error can be made arbitrarily small by including more terms in the summation over m (Appendix C). The third term $\varepsilon_{r,\,\mathrm{mpath}}$ is the error incurred by approximating arbitrarily multipath delays with uniformly delayed versions of $q(t)$. The uniform delays are multiples of $1/B$, so by choosing B sufficiently large, and by including more terms in the sum, we can approximate $q(t-\tau_l)$ arbitrarily well using $q(t-m/B)$, $m=0,1,\ldots,L$ (Appendix D). We prove inequality (15) in Appendix E.

In *sparse* multipath environments where some of the channel coefficients in H_{pml} are zero, the canonical representation as (6) may suffer from overparametrization. This problem can be mitigated by adding an algorithm which tracks the subset of "nonzero" channel coefficients, at the expense of increased complexity. An example of this is "RAKE finger tracking" in IS-95 where dominant T_c-spaced multipath delays are tracked [13].

C. Reconstruction Error for DS-CDMA Systems

We now focus on the special case of DS-CDMA systems employing spread-spectrum signaling waveforms $q(t)$ of the form

$$q(t) = \sum_{i=0}^{N-1} c_i v(t-iT_c)/C, \qquad 0 \le t < T \tag{16}$$

where $\{c_i\}$ is the spreading sequence of length N, $v(t)$ is the chip waveform of duration T_c, and C is a normalization constant which ensures $q(t)$ has *unit* energy. Since the spreading sequence has approximately flat spectral magnitude, the bandwidth B of $q(t)$ is solely determined by the bandwidth of $v(t)$, which is inversely proportional to T_c. As noted in the previous section, the definition of B affects the accuracy of the canonical representation.

We will consider bandwidth definitions of the form $B \approx \mathcal{O}/T_c$, where $\mathcal{O}$ is termed a chip rate *oversampling* factor, typically 1, 2, 4, or 8.[7] We assume the *discrete multipath channel* model given in (5). The choice of $\mathcal{O}$ and the shape of the chip waveform $v(t)$ can have a significant effect on the reconstruction error $\varepsilon_{r,\,\mathrm{MIN}}$. Clearly, we would like to select a $v(t)$ whose energy is concentrated around DC since $\varepsilon_{r,\,\mathrm{MIN}}$ is proportional to the energy of $q(t)$ outside the frequency range $|f| \le W/2$ (see Appendix D). In this paper, we use the class of *raised-cosine* chip waveforms and show that by sufficient oversampling (a maximum of 8), the reconstruction error $\varepsilon_{r,\,\mathrm{MIN}}$ can be made negligible. Define $v(t)$, as given in the equation at the bottom of the page, where α is the *roll-off factor*. Notice that $\alpha = 0$ generates a rectangular chip waveform. As α increases, the main lobe of the spectrum becomes wider, but the side lobe levels are smaller. Hence, we expect $\varepsilon_{r,\,\mathrm{MIN}}$ for $\mathcal{O}=1$ to increase as α increases due to the broadening mainlobe. However, for large α, $\varepsilon_{r,\,\mathrm{MIN}}$ should decrease more rapidly with increasing $\mathcal{O}$, because the sidelobes are smaller. These properties are shown below and illustrated with examples in Section V.

It is instructive to look at the reconstruction error associated with a single multipath temporal channel $h(t)=\delta(t-\tau_1), \tau_1 \in [0,T_c]$ for different α. To illustrate the error a length 31 M-sequence is used. In this case, the canonical basis is of the form $\{q(t-l/B)\}$ with $l=0,1,\ldots,L$ and the canonical channel parameter computation follows from Section II-B. The reconstruction error for roll-off factor of $\alpha=0$ can be easily obtained in closed form. Let $s(t)=q(t-\tau_1), \tau_1 \in (k/B, k+1/B)$, where $k=0,1,\ldots$ for rectangular chip waveform and $B=\mathcal{O}/T_c$. For simplicity, we use a rectangular chip waveform. It can be shown from (13) that due to the linearity of $c(\tau_1)=\int q(t)q(t-\tau_1)\,dt$ with respect to τ_1, the canonical channel parameters $H_{00l}=0$ for $l \ne k, k+1$. Without loss of generality, set $k=0$ hence $\tau_1 \in [0,T_c]$. In this case

$$\mathbf{R}_w = \begin{bmatrix} 1 & 1-1/\mathcal{O} \\ 1-1/\mathcal{O} & 1 \end{bmatrix}, \quad \mathbf{d} = \begin{bmatrix} 1-\tau_1/T_c \\ 1-1/\mathcal{O}+\tau_1/T_c \end{bmatrix}.$$

It can be shown from (13) and (14) that

$$\begin{aligned} H_{000} &= 1-\mathcal{O}\frac{\tau_1}{T_c}, \quad H_{001} = \mathcal{O}\frac{\tau_1}{T_c} \\ \varepsilon_{r,\,\mathrm{MIN}} &= 2\frac{\tau_1}{T_c}\left(1-\mathcal{O}\frac{\tau_1}{T_c}\right). \end{aligned} \tag{17}$$

[7]The term oversampling implies sub-chip rate sampling of the output of the matched filter $q^*(-t)$ (Fig. 5). The effects of oversampling are further discussed in Section III.

$$v(t) = \begin{cases} 1, & 0 \le \left|t-\dfrac{T_c}{2}\right| \le \dfrac{T_c}{2}(1-\alpha) \\ 0.5\left\{1+\cos\left[\dfrac{2\pi}{T_c\alpha}\left(\left|t-\dfrac{T_c}{2}\right| - \dfrac{T_c}{2}(1-\alpha)\right)\right]\right\}, & \dfrac{T_c}{2}(1-\alpha) \le \left|t-\dfrac{T_c}{2}\right| \le \dfrac{T_c}{2} \\ 0, & \text{elsewhere} \end{cases}$$

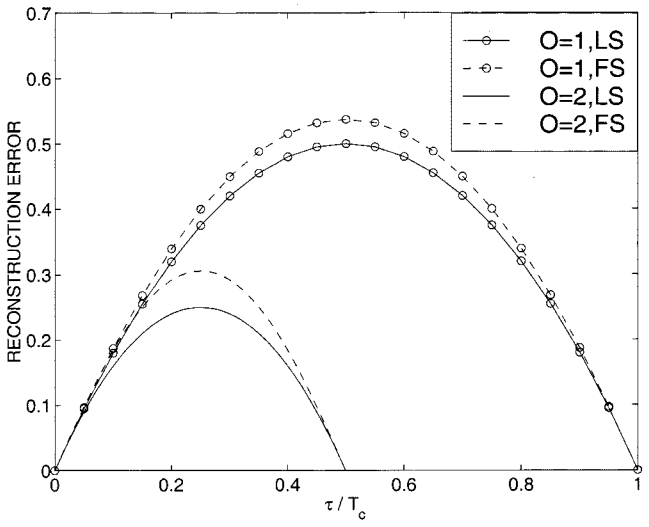

Fig. 3. Comparing reconstruction error under LS and FS methods for a single multipath case with rectangular chip waveform.

Equation (17) implies that $\varepsilon_{r,\mathrm{MIN}} \leq (1/(2\mathcal{O}))$, which approaches zero as $\mathcal{O}$ increases. Fig. 3 depicts the reconstruction error as a function of τ_1 for $\mathcal{O} = 1, 2$ with $\{H_{000}, H_{001}\}$ computed using least squares and truncated Fourier series (Appendix A) methods.

Fig. 4 shows $\varepsilon_{r,\mathrm{MIN}}$ as a function of τ_1. Notice that for a given oversampling factor $\mathcal{O}$, local maxima occur exactly at the middle of two basis function delays. For $\alpha = 0$, only the two basis functions adjacent to τ_1 contribute to $\hat{s}(t)$ due to the linearity of the rectangular waveform's temporal correlation. This is not true with $0 < \alpha \leq 1$. In general, all basis functions will contribute to the canonical representation, except when $\tau_1 = l/B$. The effect of oversampling factor $\mathcal{O}$ and roll-off factor α on reconstruction error for general frequency-selective channels is discussed in Appendix D. The oversampling factor $\mathcal{O}$ induces a tradeoff between complexity and representation error $\varepsilon_{r,\mathrm{MIN}}$. The error is directly related to symbol error as discussed in Section IV. When $\mathcal{O} = 1$, choosing $\{\varphi_p\}$ as in (8) gives a set of approximately orthonormal set of basis functions $\{\mathbf{q}_{pml}(t)\}$,[8] albeit at the expense of a loss of accuracy in the representation (6) in the case of arbitrary multipath delays. The accuracy of (6) can be improved by increasing the oversampling factor $\mathcal{O}$, although at the expense of losing orthogonality of the basis functions $\{\mathbf{q}_{pml}(t)\}$.

III. Space–Time Receiver Structure

Consider the discrete multipath channel described in (5). For simplicity in receiver design, we assume $T_m \ll T$, which is typical in mobile wireless environments and implies negligible intersymbol interference (ISI).[9] Conventional coherent space–time receivers, such as those proposed in [1], are based on the *ideal* test statistic

$$Z = \mathrm{Re}\left\{\sum_{l=1}^{L_T} \hat{\beta}_l^* \langle \mathbf{r}(t), \mathbf{a}(\hat{\phi}_l) e^{j2\pi\theta_l t} q(t - \hat{\tau}_l)\rangle\right\} \qquad (18)$$

[8]Due to the correlation properties of the spreading sequence.

[9]Large delay spreads for which ISI is not negligible can be accommodated by jointly decoding a frame of symbols.

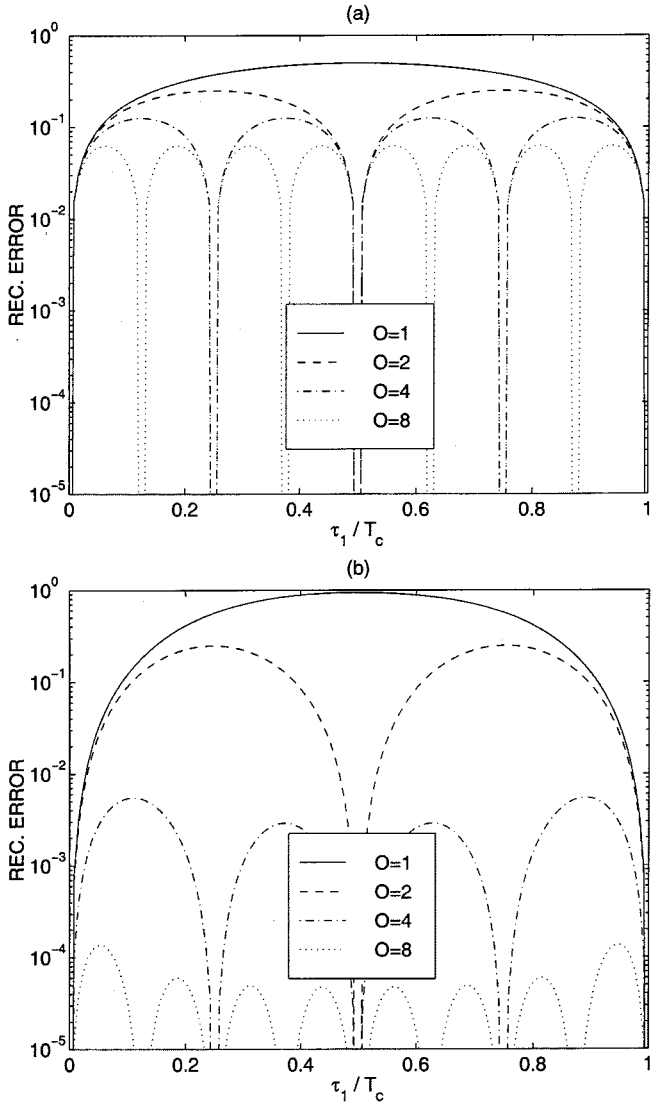

Fig. 4. ε_r as a function of τ_1 for (a) $\alpha = 0$ and (b) $\alpha = 1$.

which requires estimates of the DOAs ϕ_l, delays τ_l, and fading coefficients β_l of each multipath component. The detected symbol is given by $\mathrm{sgn}(Z)$. This receiver performs matched-filtering to all the multipath components, resulting in high complexity in a dense multipath environment. Furthermore, the performance depends on the quality of the DOA, delay, and channel parameter estimates. Even if joint angle-delay estimation frameworks [1], [14] are employed, a large number of observations and relatively complex algorithms are necessary to obtain accurate parameter estimates for the conventional receiver.

In Section II, we have shown that a space–time signal $\mathbf{s}(t)$ in (4) can be represented with arbitrary accuracy using the canonical representation. This suggests that all the signal processing in the receiver can be performed in the canonical channel coordinates. The canonical channel coordinates have lower dimensionality than the original signal space. The representation (6) also provides a framework for space–time processing that eliminates the need for DOA and delay estimates. This results in significant reduction of receiver complexity and robustness against parameter estimation errors. In addition, our approach fully accounts

for fast fading effects and in fact exploits Doppler effects for additional diversity compared to conventional receivers [5], [9].

In this paper, we develop space–time single-user receivers for binary signaling—both coherent antipodal and noncoherent orthogonal signaling are considered. Recall that the delay spread T_m is assumed to be sufficiently small ($T_m \ll T$) so that ISI is negligible and symbol-by-symbol detection suffices. The R-dimensional complex baseband signal within one symbol duration at the receiver is given by (1), $q(t) \in \{\pm q_0(t)\}$ for antipodal signaling and $q(t) \in \{q_1(t), q_2(t)\}$ for orthogonal signaling. We consider the discrete multipath model (5) for receivers development and analysis. The noise vector $\mathbf{n}(t)$ is assumed to be complex Gaussian with zero mean and $E\{\mathbf{n}(t)\mathbf{n}^H(t')\} = \mathcal{N}_0\delta(t-t')\mathbf{I}_{N_{\rm tot}}$, where $\mathbf{I}_K$ is a $K \times K$ identity matrix and $N_{\rm tot} = (P^+ - P^- + 1)(2M+1)(L+1)$.

A. Coherent Antipodal Signaling

The canonical representation in (6) suggests a coherent space–time matched filter receiver structure defined by the basis functions in (7). The canonical space–time receiver maps the received signal $\mathbf{r}(t)$ onto the basis functions to form the test statistic

$$Z = \mathrm{Re}\left\{\sum_{p=P^-}^{P+}\sum_{m=-M}^{M}\sum_{l=0}^{L}\hat{H}^*_{pml}\langle \mathbf{r}, \mathbf{q}_{pml}\rangle\right\} \tag{19}$$

where $\{\hat{H}_{pml}\}$ are estimates of the canonical channel coefficients.[10] In this paper, we assume perfect $\{\hat{H}_{pml}\}$ estimates are obtained by projecting a noise-free pilot signal onto the canonical subspace.

It is desirable to formulate the detection statistics in matrix form for analysis considerations. Define the array response matrices and delayed signaling waveforms vector

$$\begin{aligned}\mathbf{A}_T &\stackrel{\rm def}{=} [\mathbf{a}(\phi_1), \ldots, \mathbf{a}(\phi_{L_T})]\\ \psi_T(t) &\stackrel{\rm def}{=} [q(t-\tau_1), \ldots, q(t-\tau_{L_T}))]^T.\end{aligned} \tag{20}$$

Then, we can write $\mathbf{s}(t)$ in (5) as

$$\begin{aligned}\mathbf{s}(t) &= \mathbf{A}_T[\mathrm{diag}\{\psi_T(t)\}]\\ &\quad\cdot[\mathrm{diag}\{e^{j2\pi\theta_1 t}, \ldots, e^{j2\pi\theta_{L_T} t}\}][\beta_1, \ldots, \beta_{L_T}]^T\\ &\stackrel{\rm def}{=} \mathbf{A}_T\mathbf{Q}_T(t)\mathbf{\Theta}(t)\beta.\end{aligned}$$

The test statistics for binary antipodal signaling with coherent detection given in (19) can be written as $Z = \mathrm{Re}\{\hat{\mathbf{h}}^H\mathbf{y}\}$, where the superscript H denotes conjugate transpose, $\hat{\mathbf{h}}$ is the canonical channel parameter vector. The $N_{\rm tot} \times 1$ vector $\mathbf{y}$ of space–time matched filter outputs is expressed as

$$\begin{aligned}\mathbf{y} &= \int_0^T \mathbf{Q}_R^H(t)\mathbf{U}_R^H\mathbf{r}(t)\,dt\\ &= \left(\int_0^T \mathbf{Q}_R^H(t)\mathbf{U}_R^H\mathbf{A}_T\mathbf{Q}_T(t)\mathbf{\Theta}(t)\,dt\right)\beta b\\ &\quad+\int_0^T \mathbf{Q}_R^H(t)\mathbf{U}_R^H\mathbf{n}(t)\,dt \stackrel{\rm def}{=} \mathbf{R}_{bs}\beta b + \mathbf{w}\end{aligned} \tag{21}$$

[10]This method of generating a symbol decision statistic is known as maximal-ratio combining (MRC). While MRC is optimal in a single-user scenario, it is not near–far resistant in the presence of multiple-access interference [7], [15].

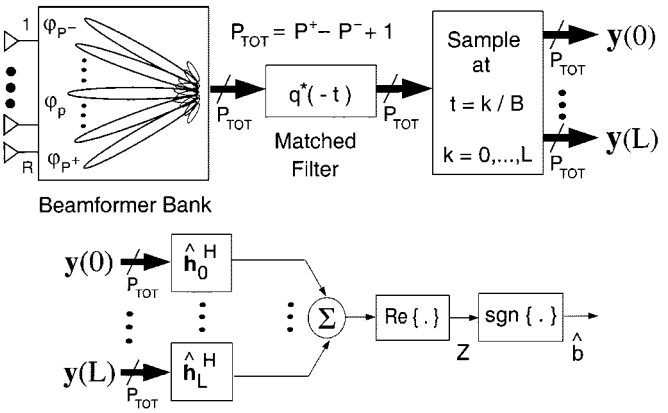

Fig. 5. Space–time RAKE receiver.

where $\mathbf{Q}_R(t)$ and $\mathbf{U}_R$ are defined in (11). The vector $\mathbf{y}$ consists of signal and noise components. For a noise-free pilot signal, the canonical channel parameter vector $\hat{\mathbf{h}}$ can be computed according to (13) by substituting the received pilot signal for $\mathbf{s}(t)$.

We note that an increase in multipath density does not affect canonical receiver performance as long as the basis functions span the signal space. Furthermore, the canonical receiver can easily adjust the number of basis functions to accommodate changes in the angular, Doppler, and delay spreads. For even modestly dense multipath environments, the complexity of the canonical receiver is substantially less than that of the conventional receiver since fewer channel parameter estimates are required and fewer matched filters need to be implemented. Furthermore, the canonical matched filter outputs can be efficiently computed via a space–time RAKE receiver structure as depicted in Fig. 5 [11].

B. Noncoherent Orthogonal Signaling

When coherent channel estimation is not practically feasible, a noncoherent detection scheme with orthogonal signaling that relies on estimates of *channel statistics* can be employed. Define $\mathbf{y} \stackrel{\rm def}{=} [\mathbf{y}_1^T\ \mathbf{y}_2^T]^T$ and $\mathbf{R}_k \stackrel{\rm def}{=} E[\mathbf{y}\mathbf{y}^H \mid q_k(t)], k = 1, 2$, where

$$\begin{aligned}\mathbf{y}_k &= \int_0^T \mathbf{Q}_{R,k}^H(t)\mathbf{U}_R^H\mathbf{r}(t)\,dt\\ \mathbf{\Gamma}_{k_1,k_2}(t) &\stackrel{\rm def}{=} \mathbf{Q}_{R,k_1}^H(t)\mathbf{U}_R^H\mathbf{A}_T\mathbf{Q}_{T,k_2}(t)\\ \mathbf{R}_k &= \begin{bmatrix}\mathbf{R}_k(1,1) & \mathbf{R}_k(1,2)\\ \mathbf{R}_k(2,1) & \mathbf{R}_k(2,2)\end{bmatrix} + \mathcal{N}_0\mathbf{R}_w\\ \mathbf{R}_k(k_1,k_2) &= \iint \mathbf{\Gamma}_{k_1,k}(t)\mathbf{R}_f(t-s)\mathbf{\Gamma}_{k_2,k}^H(s)\,dt\,ds\\ \mathbf{R}_w &\stackrel{\rm def}{=} \begin{bmatrix}\mathbf{R}_w(1,1) & \mathbf{R}_w(1,2)\\ \mathbf{R}_w(2,1) & \mathbf{R}_w(2,2)\end{bmatrix}\\ \mathbf{R}_w(k_1,k_2) &\stackrel{\rm def}{=} \int \mathbf{Q}_{R,k_1}^H(t)\mathbf{U}_R^H\mathbf{U}_R\mathbf{Q}_{R,k_2}(t)\,dt\\ \mathbf{R}_f(t-s) &\stackrel{\rm def}{=} E[\mathbf{\Theta}(t)\beta\beta^H\mathbf{\Theta}^H(s)]\\ &= \mathrm{diag}\left\{E|\beta_1|^2E(e^{j2\pi\theta_1(t-s)}), \ldots,\right.\\ &\qquad\left. E|\beta_{L_T}|^2E\left(e^{j2\pi\theta_{L_T}(t-s)}\right)\right\}\end{aligned}$$

for $k, k_1, k_2 \in \{1, 2\}$. All the matrices involved in the computation of $\mathbf{y}_k, \mathbf{R}_k, (k = 1, 2)$, are defined in Sections II-B and III-A

where the subscript k denotes the temporal basis correlation for symbol k. If $\mathbf{R}_f(t-s)$ is known, the optimal noncoherent detector computes the log-likelihood ratio $\ell(\mathbf{y}) = \mathbf{y}^H(\mathbf{R}_1^{-1} - \mathbf{R}_2^{-1})\mathbf{y}$ and compares it to a threshold [16]. If the estimate of $\mathbf{R}_f(t-s)$ cannot be obtained, an equal-gain square-law combining detector can be used [7].

IV. Performance Analysis

For performance analysis, we assume a discrete WSSUS multipath channel model in (5) with sufficiently slow fading so that Doppler effects are negligible. This is just the special case of the formulation in Section III with $\theta_l = 0$ in (20) over one symbol duration.

A. Symbol-Error Probability

The performance of ideal and canonical receivers is compared based on the *average* symbol-error probability (P_e) assuming perfect estimates of all multipath parameters $\{\hat{\beta}_l, \hat{\phi}_l, \hat{\tau}_l\}$ for the ideal receiver, and canonical channel coefficients $\{\hat{H}_{p0l}\}$ for the canonical receiver. From (5) and (21), the symbol test statistics of the canonical receiver in (19) can be written as

$$Z = \mathrm{Re}\{\hat{\mathbf{h}}^H \mathbf{R}_{bs}\beta b + \mathbf{h}^H \mathbf{w}\} \tag{22}$$

where $\mathbf{w} = \int_0^T \mathbf{Q}_R(t)\mathbf{A}_R^H \mathbf{n}(t)\,dt$ and $E[\mathbf{w}\mathbf{w}^H] = \mathcal{N}_0\mathbf{R}_w$ with $\mathbf{R}_w$ defined in (14). From (13), $\hat{\mathbf{h}} = \mathbf{R}_w^{-1}\mathbf{R}_{bs}\beta$. Hence, (22) can be written as

$$Z = \beta^H \mathbf{R}_{bs}^H \mathbf{R}_w^{-1}\mathbf{R}_{bs}\beta b + \mathrm{Re}\left\{\beta^H \mathbf{R}_{bs}^H \mathbf{R}_w^{-1}\mathbf{w}\right\}. \tag{23}$$

Assuming equiprobable binary symbols, the P_e given the fading vector β is[11]

$$P_e(\beta) = \mathcal{Q}\left(\sqrt{\frac{2}{\mathcal{N}_0}\beta^H \mathbf{R}_{bs}^H \mathbf{R}_w^{-1}\mathbf{R}_{bs}\beta}\right). \tag{24}$$

Some insight can be gained from (24). Define $\mathbf{R}_T = \int_0^T \mathbf{Q}_T(t)\mathbf{A}_T^H\mathbf{A}_T\mathbf{Q}_T(t)\,dt$. From (14), it follows that the reconstruction error given β can be written as:

$$\varepsilon_{r,\,\mathrm{MIN}}(\beta) = \beta^H\left(\mathbf{R}_T - \mathbf{R}_{bs}^H\mathbf{R}_w^{-1}\mathbf{R}_{bs}\right)\beta. \tag{25}$$

Hence, (24) can be written as

$$P_e(\beta) = \mathcal{Q}\left[\sqrt{\frac{2}{\mathcal{N}_0}\beta^H\mathbf{R}_T\beta\left(1 - \frac{\varepsilon_{r,\,\mathrm{MIN}}(\beta)}{\beta^H\mathbf{R}_T\beta}\right)}\right]. \tag{26}$$

Since P_e is obtained by averaging (24) over β, it can be seen from (26) that (by the monotonicity of $\mathcal{Q}(\cdot)$ and expectation) P_e is an increasing function of $\varepsilon_{r,\,\mathrm{MIN}}(\beta)$. This is intuitively satisfying since $\varepsilon_{r,\,\mathrm{MIN}}(\beta)/\beta^H\mathbf{R}_T\beta$ is the relative energy loss in the canonical signal representation with respect to the total received signal energy $\beta^H\mathbf{R}_T\beta$. This energy loss contributes to decision error.

Assuming β is a complex Gaussian random vector with zero mean (the Rayleigh fading model) and $E[\beta\beta^H] = \mathcal{E}\mathbf{I}_{L_T}/(\mathcal{N}_0 L_T)$,[12] where $\mathcal{E}$ is the total received energy, P_e can be obtained as follows:[13]

$$P_e = \frac{1}{2}\sum_{l=1}^{N_{\mathrm{tot}}}\prod_{i=1,i\neq l}^{N_{\mathrm{tot}}}\frac{\lambda_l}{\lambda_l - \lambda_i}\left(1 - \sqrt{\frac{\rho\lambda_l}{\rho\lambda_l + 1}}\right) \tag{27}$$

where $\rho = \mathcal{E}/(\mathcal{N}_0 L_T)$ and $\{\lambda_l\}$ are the nonzero eigenvalues of the signal matrix $\mathbf{\Phi} \stackrel{\mathrm{def}}{=} \mathbf{R}_{bs}^H\mathbf{R}_w^{-1}\mathbf{R}_{bs}$.[14] Note that the effects of reconstruction error and diversity on symbol-error rate are coupled in (27). Basically, reconstruction error $\varepsilon_{r,\,\mathrm{MIN}}$ represents the amount of signal energy captured by receiver, while diversity represents the number of independent signal copies available at the receiver due to the channel scattering. The number of *effective diversity* and corresponding energy distribution are determined by the number of significant eigenvalues and eigenvalue distribution of the signal matrix $\mathbf{\Phi}$.

The P_e of the ideal receiver can analyzed in the same manner since its test statistic Z is a special case of (23), where $\mathbf{R}_{bs} = \mathbf{R}_w = \mathbf{R}_T$; hence $\mathbf{\Phi} = \mathbf{R}_T$. The P_e for a noncoherent receiver can be obtained in a similar manner. In particular, by using the eigendecomposition and adopting the approach in [7], a closed-form expression for P_e can also be derived.

B. Diversity Gain

Quantifying the diversity gain from P_e is not a clear-cut matter since the effect of diversity and energy loss on P_e are not separable, as apparent from (27). We choose to define the diversity gain of a space–time receiver with a signal matrix $\mathbf{\Phi}$ as follows:

$$D_G = \frac{P_e(\text{receiver})}{\frac{1}{2}\left(1 - \sqrt{\frac{\rho\,\mathrm{tr}(\mathbf{\Phi})}{1+\rho\,\mathrm{tr}(\mathbf{\Phi})}}\right)} \tag{28}$$

where ρ is as in (27) and $\mathrm{tr}(\mathbf{M})$ is the trace of matrix $\mathbf{M}$. The denominator is just the symbol-error probability of a single-path Rayleigh fading channel with the same amount of received signal energy as that remaining after the space–time matched filtering operation(ideal or canonical). We will see in the next section that the proposed receivers capture virtually all diversity available in the received signal. In particular, the loss in the diversity gain decreases as the oversampling factor $\mathcal{O}$ is increased and at $\mathcal{O} = 8$ the loss is virtually negligible.

V. Examples

As noted in Section III, the canonical receiver only requires estimates of the canonical channel coefficients, while the ideal receiver requires estimates of *all* multipath, DOAs, time delays, and fading parameters. For comparison purposes, we assume all parameters required are estimated perfectly. Although unrealistic, this assumption provides an upper bound on performance. Coherent detection and binary antipodal signaling are assumed. A length-31 M sequence serves as the spreading code, and P_e

[11] $\mathcal{Q}(x) = (1/\sqrt{2\pi})\int_x^\infty e^{-(t^2/2)}\,dt$.

[12] Uniform power uncorrelated scatterer [7], a commonly used model.

[13] Using [7, pp. 801–802] and the Karhunen–Loeve expansion of the random vector $\mathbf{R}_w^{-1/2}\mathbf{R}_{bs}\beta$.

[14] $\mathbf{\Phi} \stackrel{\mathrm{def}}{=} \mathbf{R}_{bs}^H\mathbf{R}_w^{-1}\mathbf{R}_{bs}E[\beta\beta^H]$ if uncorrelated scatterer model is relaxed.

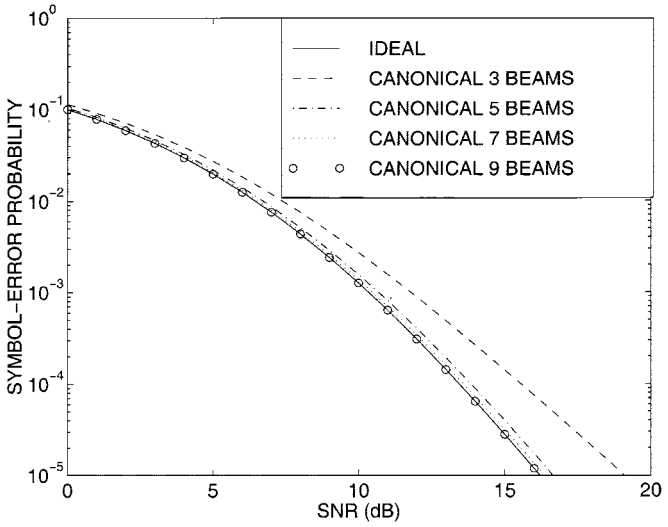

Fig. 6. Coherent space-only processing: ideal versus canonical with different number of beams.

as a function of $\mathrm{SNR}(=\mathcal{E}/\mathcal{N}_0)$ is used as the performance measure.

A. Example 1. Coherent Space-Only Processing

A nine-element uniform linear array is used with half-wavelength spacing. A total of 21 multipath arrivals with DOAs uniformly distributed on $[-\pi/10, \pi/10]$ is assumed with zero delay spread ($T_m = 0$). The canonical receiver is based on up to nine beams with directions chosen according to (8) to obtain $\varphi_k \in \{0, \pm 0.07\pi, \pm 0.15\pi, \pm 0.23\pi, \pm 0.35\pi\}$. Fig. 6 depicts the performance of the conventional and several canonical receivers based on different numbers of beam directions. The receiver with "three beams" uses the directions $\{0, \pm 0.07\pi\}$, "five beams" uses $\{0, \pm 0.07\pi, \pm 0.15\pi\}$, "seven beams" uses $\{0, \pm 0.07\pi, \pm 0.15\pi, \pm 0.23\pi\}$, while "nine beams" use all nine φ_k. The three-beam canonical receiver experiences a 2.5-dB SNR loss at $P_e = 10^{-4}$ since the beams with directions $\{\pm 0.07\pi\}$ do not span the space corresponding to the angular spread of the multipath ($|\phi| < \pi/10$). However, as suggested by the canonical signal model, five beams are sufficient to represent the given angle spread, as evident from the nearly identical performance of the canonical receiver with five, seven, or nine beams and the conventional receiver exactly matched to the DOAs. Note that the conventional receiver requires estimates of 21×2 DOA and fading parameters and forms 21 beams, whereas canonical receiver requires estimates of at most nine channel parameters and forms at most nine beams.

B. Example 2. Coherent Space–Time Processing with Raised-Cosine Chip Waveform of Different Roll-Off Factors α

In this example, symbol-error probability for roll-off factors α of 0, 1 are computed. A four-element uniform linear array with a half-wavelength spacing is used and a dense multipath environment with a total of 11×64 scatterers distributed evenly over $[-\pi/10, \pi/10] \times [0, 3.9375T_c]$ is simulated. The canonical representation samples at DOAs $\{\pm 0.08\pi, \pm 0.27\pi\}$ with $\mathcal{O} = 1, 2, 4, 8$ for each α.

Fig. 7(a) and (b) compares the performance of the conventional (ideal) and canonical receivers. At a symbol-error probability 10^{-4}, the canonical receiver with a roll-off factor of $\alpha = 0$ is within 0.5 dB of the ideal receiver for $\mathcal{O} = 4$ or 8, and this gap decreases with increasing $\mathcal{O}$. Note that the canonical receiver delivers this near-optimal performance at a substantially reduced complexity. The ideal receiver requires $11 \times 64 \times 3$ estimates of $(\phi_l, \tau_l, \beta_l)$, and computation of 11×64 matched space–time filter outputs. In contrast, the canonical receiver for $\mathcal{O} = 8$ only requires estimates of 4×33 coefficients $\hat{H}_{p0l}$ and computation of 4×33 matched filter outputs. Similar complexity savings also occur for $\alpha = 1$ with improved performance (compared to that for $\alpha = 0$) as demonstrated next. Notice that for raised-cosine with $\alpha = 0$ at symbol-error probability of 10^{-4}, a 2.3-dB SNR loss occurs for $\mathcal{O} = 1$ and 0.3 dB for $\mathcal{O} = 4$. For $\alpha = 1$, the canonical receiver experiences a loss of 4 dB for $\mathcal{O} = 1$ and virtually no loss for $\mathcal{O} = 4$. The increased SNR loss at $\mathcal{O} = 1$ for roll-off factor of $\alpha = 1$ occurs because the spectral main lobe is twice as wide as that for roll-off factor of $\alpha = 0$. However, the side lobe magnitudes decay much faster for $\alpha = 1$, resulting in virtually no SNR loss as compared with that for $\alpha = 0$.

The diversity gain D_G for the above receiver structures above are computed and depicted in Fig. 7(c) and (d). As expected, the loss in diversity gain with respect to the ideal receiver become smaller as the oversampling factor $\mathcal{O}$ is increased. The effect of roll-off factor α on diversity gain is similar to that on symbol-error probability.

The above examples demonstrate that P_e of canonical receivers approach those of the ideal receiver within a *practical range* of SNR (0–15 dB) as the oversampling factor $\mathcal{O}$ and/or raised-cosine roll-off factor α increase. In fact, the difference in P_e can be made arbitrarily small since the reconstruction error can also be made arbitrarily small. This indicates that the canonical coordinate signal representation is able to capture essentially all the signal energy arriving at the receiver. The last example indicates that these receivers capture all the essential diversity that are contained in the received space–time signal.

VI. Discussion and Conclusions

In this paper, we have introduced a parsimonious canonical representation for arbitrary time-varying spatio-temporal channels. The representation exploits the fact that the underlying signal space possesses finite degrees of freedom due to the finite duration and essentially finite bandwidth of signaling waveform and finite aperture of sensor array. The representation has been shown to capture all the essential degrees of freedom and energy that are contained within the signal. This representation is used to design wireless space–time receivers that eliminate the need for delay, Doppler, and DOA parameter estimation. The resulting receivers attain near-optimal performance, with substantially less complexity than existing designs, particularly in dense multipath environments. The number of parameters in the canonical representation is independent of the number of multipaths and depends only on the angle, delay, and Doppler spreads of the channel.

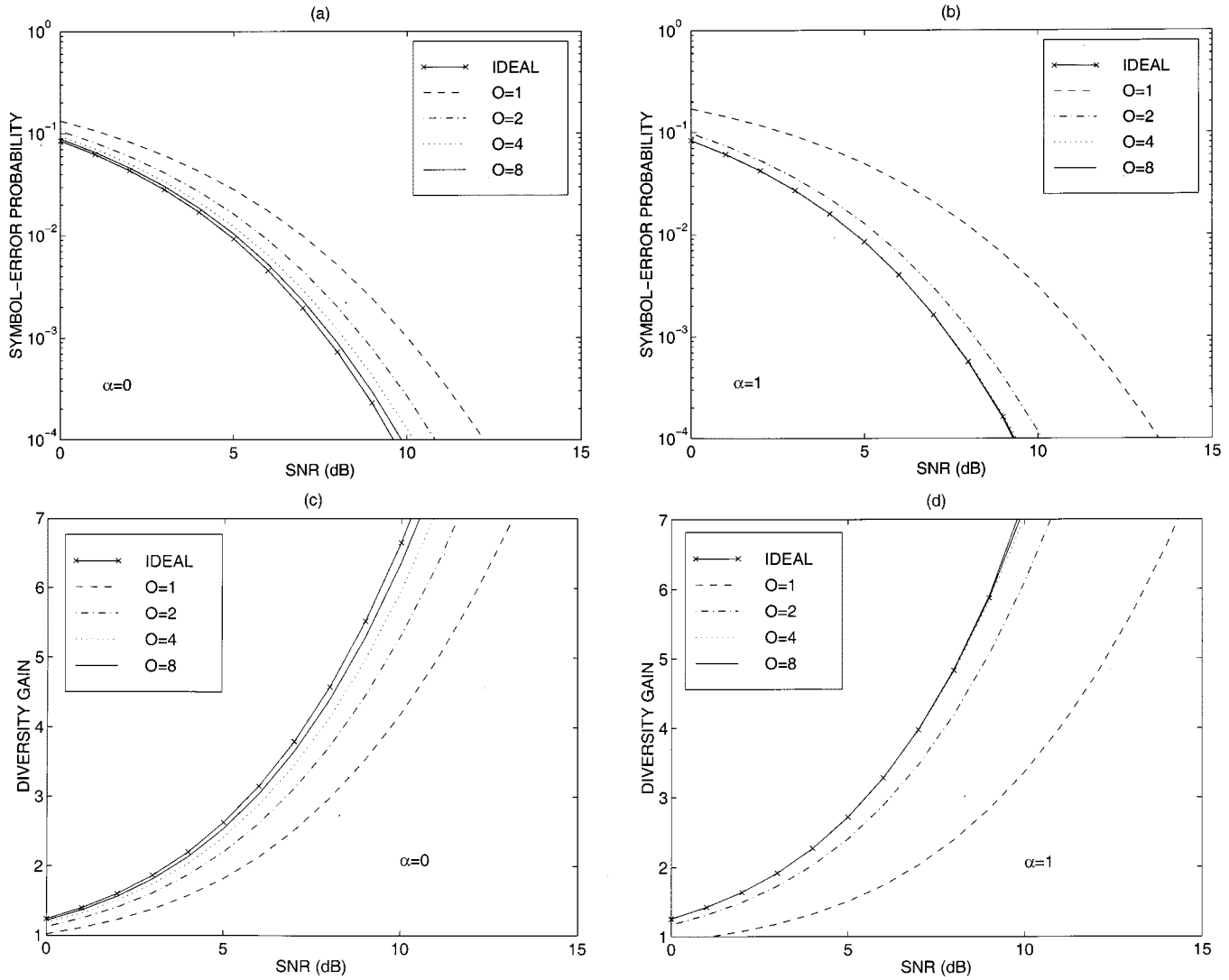

Fig. 7. Coherent space–time processing raised-cosine chip waveform: ideal versus canonical with (a) P_e for $\alpha = 0$ (rectangular), (b) P_e for $\alpha = 1$, (c) diversity gain for $\alpha = 0$, and (d) diversity gain for $\alpha = 1$.

The parsimonious nature of the proposed canonical coordinate representation simplifies a number of problems in mobile wireless communication. In the case of time-only processing, the representation has been exploited for diversity processing, interference suppression, and timing acquisition [5], [17], [9], [18]. In a multiuser context, the canonical representation provides a natural framework for tailoring receiver complexity to a desired level of performance. We are currently investigating the use of the canonical representation in several aspects of multiuser spatio-temporal receiver design, including interference suppression [15], [19], channel estimation, and timing acquisition.

APPENDIX A
PROOF OF CANONICAL SIGNAL REPRESENTATION THEOREM

To prove (6), we devise a method to compute the canonical channel parameters H_{pml}. First, we derive a *strictly* band-limited approximation of $\mathbf{s}(t)$. Then, the Fourier series of the approximation is truncated to leave out the terms that are 'sufficiently outside' the delay, Doppler, and angle spread. Due to its time-limited and essentially band-limited nature, $x(\phi, t)$ admits a representation[15] [5]

$$x(\phi,t) \approx \sum_{m=-M}^{M} \sum_{l=0}^{L} \hat{F}_{ml}(\phi) e^{((j2\pi mt)/M)} q\left(t - \frac{l}{B}\right)$$

$$\hat{F}_{ml}(\phi) = \int_0^{T_m} \int_{-B_d}^{B_d} H(\phi,\theta',\tau') e^{-j\pi((m/T)-\theta')T} \times \operatorname{sinc}\left(\left(\frac{m}{T} - \theta'\right)T\right) \times \operatorname{sinc}\left(\left(\frac{l}{B} - \tau'\right)B\right) d\theta'\, d\tau'$$

where $L = \lceil T_m B \rceil$ and $M = \lceil T B_d \rceil$. Then, (4) can be written as

$$\mathbf{s}(t) \approx \sum_{m=-M}^{M} \sum_{l=0}^{L} e^{\frac{j2\pi mt}{M}} q\left(t - \frac{l}{B}\right) \int_{S^-}^{S^+} \hat{F}_{ml}(\phi)\mathbf{a}(\phi)\, d\phi.$$

[15] $\operatorname{sinc}(x) = \sin(\pi x)/(\pi x)$.

By choosing $\{\varphi_p\}_{p=1}^R$ such that $\{\mathbf{a}(\varphi_p)\}_{p=1}^R$ are linearly independent, $\text{span}(\{\mathbf{a}(\varphi_p)\}_{p=1}^R) = \mathcal{C}^R$, hence there exists coefficients v_{pml} such that

$$\int_{S^-}^{S^+} \hat{F}_{ml}(\phi)\mathbf{a}(\phi)\,d\phi = \sum_{p=1}^{R} v_{pml}\mathbf{a}(\varphi_p). \tag{29}$$

In particular, if $\{\varphi_p\}$ are chosen so that $\{\mathbf{a}(\varphi_p)\}$ are orthogonal, then

$$v_{pml} = \mathbf{a}^H(\varphi_p)\int_{S^-}^{S^+} \hat{F}_{ml}(\phi)\mathbf{a}(\phi)\,d\phi, \qquad p = 1,\ldots,R.$$

Otherwise

$$[v_{1ml},\ldots,v_{Rml}]^T = \left(\mathbf{U}_R^H\mathbf{U}_R\right)^{-1}\mathbf{U}_R^H\int_{S^-}^{S^+} \hat{F}_{ml}(\phi)\mathbf{a}(\phi)\,d\phi$$

where $\mathbf{U}_R$ is defined in (12). It is shown in Appendix B for uniform linear array with $\{\varphi_p\}_{p=1}^R$ chosen according to (8) that terms outside $p = P^-,\ldots,P^+$ are small. Hence, (6) follows.

While this method highlights the idea behind canonical signal representation, it is not optimal in the least square sense. As demonstrated in Appendix B, the error in the spatial domain originates from the truncation of the summation in (29). The magnitude of the error depends on the contribution of the excluded array response vectors due to a source from an arbitrary direction in $[S^-, S^+]$. Since the excluded response vectors $\mathbf{a}(\phi)$ are associated with directions $\phi \notin [S^-, S^+]$, it is the sidelobe levels of the array response that determine the truncation error.

Appendix B
Upper Bound for $\varepsilon_{r,\,\text{angle}}$—Angle Only

Consider the angle-only case where $\mathbf{s} = \int_{S^-}^{S^+} h(\phi)\mathbf{a}(\phi)\,d\phi = h(\phi_*)\mathbf{a}(\phi_*)S_\Delta$ for some $\phi_* \in (S^-, S^+), S_\Delta \stackrel{\text{def}}{=} S^+ - S^-$ by mean value theorem. For simplicity, we use uniform linear array (ULA) with $\{\varphi_p\}_{p=1}^R$ given in (8), which corresponds to orthogonal set of $\{\mathbf{a}(\varphi_p)\}_{p=1}^R$. Define $\mathcal{S} \stackrel{\text{def}}{=} \{P^-,\ldots,P^+\}$. Given $\phi_* \in [\varphi_n, \varphi_{n+1})$ (hence $\{n, n+1\} \subset \mathcal{S}$), it follows from (8) that there exists $0 < \delta_0 < 2$ for $p \notin \mathcal{S}$ such that

$$\Delta_R(n,p) \stackrel{\text{def}}{=} \sin(\varphi_p) - \sin(\phi_*) = \frac{1}{R}|\delta_0 + 2(n-p)|.$$

Then, the corresponding energy in the canonical channel parameter $\hat{H}_p$ is

$$\begin{aligned}|\hat{H}_p|^2 &= |h(\phi_*)S_\Delta\mathbf{a}^H(\varphi_p)\mathbf{a}(\phi_*)|^2\\ &= \left|h(\phi_*)S_\Delta\frac{\sin\left(\frac{\pi}{2}R\Delta_R(n,p)\right)}{\sin\left(\frac{\pi}{2}\Delta_R(n,p)\right)}\right|^2\\ &= |h(\phi_*)S_\Delta|^2\frac{\sin^2(\pi\delta_0/2)}{\sin^2(\Delta_R(n,p))}.\end{aligned} \tag{30}$$

It is apparent $|\hat{H}_p|^2$ are small for $p \notin \mathcal{S}$ as they correspond to the sidelobe energy. Hence

$$\begin{aligned}\varepsilon_{r,\,\text{angle}} &= \left\|\sum_{p\notin\mathcal{S}}\hat{H}_p\mathbf{a}(\varphi_p)\right\|_{\text{ST}}^2 = \sum_{p\notin\mathcal{S}}|\hat{H}_p|^2\\ &= \sin^2\left(\frac{\pi}{2}\delta_0\right)|h(\phi_*)S_\Delta|^2\sum_{p\notin\mathcal{S}}\frac{1}{\sin^2(\Delta_R(n,p))}\end{aligned}$$

which can be made arbitrarily small by including more terms in the representation. When all R terms are used, $\varepsilon_{r,\,\text{angle}} = 0$.

Appendix C
Upper Bound for $\varepsilon_{r,\,\text{doppler}}$—Doppler Only

In the Doppler-only case, $s(t) = h(t)q(t)$ and $h(t) = \int_{-B_d}^{B_d} H(\theta)e^{j2\pi\theta t}$. Then, the canonical channel parameters

$$\begin{aligned}\hat{H}_m &= \int_{-B_d}^{B_d} H(\theta)e^{j\pi(\theta - m/T)}\text{sinc}((\theta - m/T)T)\,d\theta\\ &= 2B_dH(v_*)e^{j\pi(v_*-m)}\text{sinc}(v_* - m)\end{aligned} \tag{31}$$

for some $v_* \in (-B_dT, B_dT)$. Here, differentiability of $H(v)$ in $(-B_dT, B_dT)$ is assumed and mean value theorem is used for the second equality. It can be seen from (31) that most energy is contained in $|m| \le \lceil B_dT\rceil$, which corresponds to the main lobe of the 'sinc' function. The reconstruction error originates from the truncation of the series. We have

$$\begin{aligned}&\varepsilon_{r,\,\text{doppler}}\\ &= 4\int_0^T\left|\sum_{m=M+1}^{\infty}\hat{H}_me^{j2\pi((mt)/T)}\right|^2dt\\ &= 4\sum_{m=M+1}^{\infty}\sum_{m'=M+1}^{\infty}\hat{H}_m\hat{H}_{m'}^*\int_0^T e^{j((2\pi)/T)(m-m')t}dt\\ &= 4T\sum_{m=M+1}^{\infty}|\hat{H}_m|^2\\ &= \underbrace{\left(\frac{4B_d\sqrt{T}|H(v_*)|\sin(\pi v_*)}{\pi}\right)^2}_{\mathcal{K}^2_{\text{doppler}}}\times\sum_{m=M+1}^{\infty}\frac{1}{(m-v_*)^2}\\ &\le \int_{M+1}^{\infty}\frac{\mathcal{K}^2_{\text{doppler}}\,dx}{(x-v_*)^2} = \frac{\mathcal{K}^2_{\text{doppler}}}{M+1-v_*}.\end{aligned}$$

Then, as M is increased above $\lceil B_dT\rceil$, the reconstruction error goes to zero.

Appendix D
Upper Bound for $\varepsilon_{r,\,\text{mpath}}$—Multipath Only

Consider the case when $M = 0$ and $R = 1$ (no Doppler shift or spatial diversity). In particular, we would like to investigate the effect of oversampling factor $\mathcal{O}$ and roll-off factor on the reconstruction error $\varepsilon_{r,\,\text{mpath}}$ (see Section II-C). The reconstruction error in this case is upper bounded by the error in Fourier

series expansion [5] which consists of the error due to bandwidth truncation of $s(t)$ ($\varepsilon_{r,bw}$) and Fourier series truncation of the bandwidth-truncated signal $s_B(t)$ ($\varepsilon_{r,\,\mathrm{trunc}}$). It follows from triangular inequality property of the space–time norm defined in Section II-B that $\sqrt{\varepsilon_{r,\,\mathrm{mpath}}} \le \sqrt{\varepsilon_{r,bw}} + \sqrt{\varepsilon_{r,\,\mathrm{trunc}}}$. But

$$\begin{aligned}\varepsilon_{r,bw} &= \int |s(t)-\hat{s}(t)|^2\,dt \\ &\le 2 \sup_{f\in[B/2,\infty)} |H(f)|^2 \int_{B/2}^{\infty} |Q(f)|^2\,df \\ &\stackrel{\mathrm{def}}{=} 2\bar{H}\int_{B/2}^{\infty} |Q(f)|^2\,df \end{aligned} \tag{32}$$

where $Q(f)$ is the Fourier transform of $q(t)$. Since the spreading code has an approximately flat spectrum, $\varepsilon_{r,bw} \approx 2\bar{H}N^2\int_{B/2}^{\infty}|V(f)|^2\,df$, where N is the spreading gain. For a raised-cosine chip waveform with roll-off factor α, it can be shown that for $\alpha = 0$

$$\varepsilon_{r,bw} \le 2N^2\int_{B/2}^{\infty}\frac{df}{f^2} = 8N^2\frac{T_c}{\mathcal{O}}. \tag{33}$$

For $0 < \alpha \le 1$, with $z \stackrel{\mathrm{def}}{=} (2T_c/\sqrt{K_2}\mathcal{O}\alpha)$

$$\begin{aligned}\varepsilon_{r,bw} &\le K_1\int_{B/2}^{\infty}\frac{df}{f^2\left(f^2-K_2^{-1}\alpha^{-2}\right)^2} \\ &= K_1(\sqrt{K_2}\alpha)^5\left[\frac{3}{4}\log\left(\frac{1-z}{1+z}\right)\right. \\ &\quad \left. +\frac{3}{2}z+\frac{1}{2}z^3+\frac{z^5}{2(1-z^2)}\right] \\ &= \sum_{j=2}^{\infty}\left(\frac{2T_c}{\mathcal{O}}\right)^{2j+1}\frac{K_3(j)}{\alpha^{2(j-2)}} \\ &\approx K_3(2)\left(\frac{2T_c}{\mathcal{O}}\right)^5+\frac{K_3(3)}{\alpha^2}\left(\frac{2T_c}{\mathcal{O}}\right)^7\end{aligned}$$

for some constants K_1, K_2, and a sequence $K_3(j)$ for which the above series is absolutely summable.[16] This shows that for large $\alpha, \varepsilon_{r,bw}$ decays faster with higher terms.

The bound for $\varepsilon_{r,\,\mathrm{trunc}}$ is derived as in Appendix B since by mean value theorem

$$\hat{H}_l = \int_0^{T_m} h(\tau)\mathrm{sinc}(B\tau l)\,d\tau = T_m h(\tilde{\tau})\mathrm{sinc}(B\tilde{\tau}l)$$

for some $\tilde{\tau} \in (0, T_m)$. It is apparent that for $l > \lceil T_m B\rceil$, the coefficients $\hat{H}_l$ are small. Hence

$$\begin{aligned}&\varepsilon_{r,\,\mathrm{trunc}} \\ &\quad = 4\sum_{l=L+1}^{\infty}\sum_{l'=L+1}^{\infty}\hat{H}_l\hat{H}_{l'}^*\int q\left(t-\frac{l}{B}\right)q\left(t-\frac{l'}{B}\right)dt \\ &\quad = \mathcal{C}^2\sum_{l=L+1}^{\infty}|\hat{H}_l|^2.\end{aligned} \tag{34}$$

[16]Equation (34) can be obtained from a Taylor series expansion around $z = 0$ for $z < 1$.

Such $\mathcal{C} > 0$ exists, since the autocorrelation of the spreading code is banded diagonal, i.e.,

$$\int q\left(t-\frac{l}{B}\right)q\left(t-\frac{l'}{B}\right)dt \approx 0, \qquad |l-l'| \ge BT_c. \tag{35}$$

Hence, $\mathcal{C}$ is to account for the off-diagonal terms. Then, analogous to Appendix C

$$\begin{aligned}\varepsilon_{r,\,\mathrm{trunc}} &= \underbrace{\left(\frac{2\mathcal{C}T_m|h(\tilde{\tau})|\sin(\pi B\tilde{\tau})}{\pi}\right)^2}_{\mathcal{K}^2_{\mathrm{mpath}}}\times\sum_{l=L+1}^{\infty}\frac{1}{(l-B\tilde{\tau})^2} \\ &\le \frac{\mathcal{K}^2_{\mathrm{mpath}}}{(L+1-B\tilde{\tau})}\end{aligned}$$

which can be made arbitrarily small by incorporating more terms (except for $\alpha = 0$, see Fig. 4).

Appendix E
Proof of (15)

Given an arbitrary spatio-temporal signal $\mathbf{s}(t)$ as in (4), $\varepsilon_{r,\,\mathrm{MIN}} = \|\mathbf{s}(t)-\hat{\mathbf{s}}_O(t)\|^2_{\mathrm{ST}}$, where $\hat{\mathbf{s}_O}(t)$ is the least squares optimal estimate of $\mathbf{s}(t)$ within the linear span of the space–time canonical basis. By the uniqueness of least square solution, for any $\hat{\mathbf{s}}(t) \ne \hat{\mathbf{s}}_O(t)$.

$$\begin{aligned}\sqrt{\varepsilon_{r,\,\mathrm{MIN}}} &< \|\mathbf{s}(t)-\hat{\mathbf{s}}(t)\|_{\mathrm{ST}} \\ &\le \|\mathbf{s}(t)-\hat{\mathbf{s}}_{\mathrm{angle}}(t)\|_{\mathrm{ST}}+\|\hat{\mathbf{s}}_{\mathrm{angle}}(t)-\hat{\mathbf{s}}_{\mathrm{dopp}}(t)\|_{\mathrm{ST}} \\ &\quad +\|\hat{\mathbf{s}}_{\mathrm{dopp}}(t)-\hat{\mathbf{s}}(t)\|_{\mathrm{ST}}\end{aligned} \tag{36}$$

for any $\hat{\mathbf{s}}_{\mathrm{angle}}(t), \hat{\mathbf{s}}_{\mathrm{dopp}}(t) \in \mathcal{C}^R \otimes \mathcal{L}_2$. The second inequality follows from triangular inequality property of a norm. By mean value theorem, $\mathbf{s}(t) = \mathbf{a}(\bar{\phi})x(\bar{\phi},t)S_\Delta$ for some $\bar{\phi} \in (S^-, S^+)$. Note that $\hat{\mathbf{s}}_{\mathrm{angle}}(t), \hat{\mathbf{s}}_{\mathrm{dopp}}(t)$ are arbitrary and $\hat{\mathbf{s}}(t)$ is arbitrary within the linear span of space–time canonical basis. To obtain (15), $\hat{\mathbf{s}}_{\mathrm{angle}}(t), \hat{\mathbf{s}}_{\mathrm{dopp}}(t)$, and $\hat{\mathbf{s}}(t)$ are chosen as follows:

$$\begin{aligned}\hat{\mathbf{s}}_{\mathrm{angle}}(t) &= S_\Delta x\left(\bar{\phi},t\right)\sum_p F_p\mathbf{a}(\varphi_p) \\ \hat{\mathbf{s}}_{\mathrm{dopp}}(t) &= \left[S_\Delta\sum_p F_p\mathbf{a}(\varphi_p)\right] \\ &\quad \times\int_0^{T_m} q(t-\tau)\sum_m G_m\left(\bar{\phi},\tau\right)e^{j((2\pi mt)/T)}\,d\tau \\ \hat{\mathbf{s}}(t) &= \left[S_\Delta\sum_p F_p\mathbf{a}(\varphi_p)\right] \\ &\quad \times\sum_m e^{j((2\pi mt)/T)}\sum_l J_{ml}(\bar{\phi})q\left(t-\frac{l}{B}\right).\end{aligned} \tag{37}$$

The choices above reflect three successive least square approximations of $\mathbf{s}(t)$ in angle, Doppler, and multipath domain alone, respectively. The expansion coefficients $\{F_p\}, \{G_m(\bar{\phi},\tau)\}, \{J_{ml}(\bar{\phi})\}$ are chosen such that each error term in (36) is minimized.

It can be shown from (36), (37), and Cauchy-Schwartz's inequality that

$$\|\mathbf{s}(t)-\hat{\mathbf{s}}_{\text{angle}}(t)\|_{\text{ST}}^2 = C_{\text{angle}}^2 \times \varepsilon_{r,\,\text{angle}}$$

$$\|\hat{\mathbf{s}}_{\text{angle}}(t)-\hat{\mathbf{s}}_{\text{dopp}}(t)\|_{\text{ST}}^2 \le C_{\text{doppler}}^2 \times \varepsilon_{r,\,\text{doppler}}$$

$$\|\hat{\mathbf{s}}_{\text{dopp}}(t)-\hat{\mathbf{s}}(t)\|_{\text{ST}}^2 7 \le C_{\text{mpath}}^2 \times \varepsilon_{r,\,\text{mpath}}$$

$$C_{\text{angle}}^2 = S_\Delta^2 \int |x(\bar{\phi},t)|^2\,dt$$

$$\varepsilon_{r,\,\text{angle}} = \left\| \mathbf{a}(\bar{\phi}) - \sum_p F_p \mathbf{a}(\varphi_p) \right\|_{\text{ST}}^2$$

$$C_{\text{doppler}}^2 = S_\Delta^2 \left\| \sum_p F_p \mathbf{a}(\varphi_p) \right\|_{\text{ST}}^2 \|q(t-\bar{\tau})\|_{\text{ST}}^2$$

$$\varepsilon_{r,\,\text{doppler}} = \left\| \int_{-B_d}^{B_d} H(\bar{\phi},\theta,\tau) e^{j2\pi\theta t}\,d\theta - \sum_m G_m(\bar{\phi},\tau) e^{j((2\pi m t)/T)} \right\|_{\text{ST}}^2$$

$$C_{\text{mpath}}^2 = S_\Delta^2 \left\| \sum_p F_p \mathbf{a}(\varphi_p) \right\|_{\text{ST}}^2 (2M+1)^2 T$$

$$\varepsilon_{r,\,\text{mpath}} = \max_{m\in\{-M,\ldots,M\}} \left\| \int G_m(\bar{\phi},\tau) q(t-\tau)\,d\tau - \sum_l J_{ml}(\bar{\phi}) q\left(t-\frac{l}{B}\right) \right\|_{\text{ST}}^2$$

Hence, (15) follows.

REFERENCES

[1] A. J. Paulraj and C. B. Papadias, "Space–time processing for wireless communications," *IEEE Signal Processing Mag.*, pp. 49–83, Nov. 1997.

[2] M. D. Zoltowski and D. Tseng, "Blind channel identification for narrowband digital communications based on parametric modeling of the channel impulse response," in *Proc. 35th Annu. Allerton Conf. Communications, Systems, and Computing*, 1997, pp. 503–512.

[3] M. D. Zoltowski, D. Tseng, and T. A. Thomas, "On the use of basis functions in blind equalization based on deterministic least squares," in *Proc. 31st Asilomar IEEE Conf. Signals, Systems, and Computers*, 1997, pp. 816–822.

[4] Z. Ding, "Multipath channel identification based on partial system information," *IEEE Trans. Signal Processing*, vol. 45, pp. 235–240, Jan. 1997.

[5] A. M. Sayeed and B. Aazhang, "Joint multipath-Doppler diversity in mobile wireless communications," *IEEE Trans. Commun.*, vol. 47, pp. 123–132, Jan. 1999.

[6] G. B. Giannakis and C. Tepedelenlioglu, "Basis expansion models and diversity techniques for blind identification and equalization of time-varying channels," *Proc. IEEE*, vol. 86, pp. 1969–1986, Oct. 1998.

[7] J. G. Proakis, *Digital Communications*, 3rd ed. New York: McGraw-Hill, 1995.

[8] P. A. Bello, "Characterization of randomly time-variant linear channels," *IEEE Trans. Commun. Syst.*, vol. CS-11, pp. 360–393, 1963.

[9] A. M. Sayeed, "Canonical multipath-Doppler coordinates in wireless communications," in *Proc. 36th Annu. Allerton Conf. Communication, Control and Computing*, Monticello, IL, 1998, pp. 536–545.

[10] D. Slepian, "On bandwidth," *Proc. IEEE*, vol. 64, pp. 292–300, Mar. 1976.

[11] A. M. Sayeed, E. N. Onggosanusi, and B. D. Van Veen, "A canonical space–time characterization of mobile wireless channels," *IEEE Commun. Lett.*, pp. 94–96, Apr. 1999.

[12] J. Brewer, "Kronecker products and matrix calculus in system theory," *IEEE Trans. Circuits Syst.*, vol. CAS-25, pp. 772–781, Sept. 1978.

[13] A. J. Viterbi, *CDMA: Principles of Spread Spectrum Communications*. Reading, MA: Addison-Wesley, 1995.

[14] G. G. Rayleigh and T. Boros, "Joint space–time parameter estimation for wireless communication channels," *IEEE Trans. Signal Processing*, pp. 1333–1343, May 1998.

[15] E. N. Onggosanusi, A. M. Sayeed, and B. D. Van Veen, "Canonical space–time coordinates for multiuser wireless communications," in *Proc. 1999 2nd IEEE Signal Processing Workshop on Signal Processing for Wireless Communications (SPAWC)*, 1999.

[16] L. L. Scharf, *Statistical Signal Processing*. Reading, MA: Addison-Wesley, 1991.

[17] S. Bhasyam, A. M. Sayeed, and B. Aazhang, "Time-selective signaling and reception for communication over multipath fading channels," *IEEE Trans. Commun.*, vol. 48, pp. 83–94, Jan. 2000.

[18] A. M. Sayeed and B. Aazhang, "Multiuser timing acquisition over multipath fading channels," in *Proc. 1998 Conf. Information Sciences and Systems (CISS'98)*, Princeton, NJ, 1998, pp. 642–647.

[19] E. N. Onggosanusi, A. M. Sayeed, and B. D. Van Veen, "Low complexity space–time multiuser detectors," in Proc. 1999 IEEE Wireless Communications and Networking Conf. (WCNC), 1999.

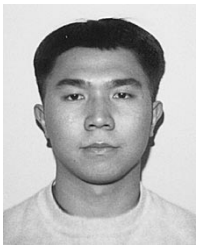

Eko N. Onggosanusi received the B.S. (with highest distinction) and M.S. degrees in electrical engineering from the University of Wisconsin–Madison in 1996 and 1998, respectively. He is currently working toward the Ph.D. degree at the University of Wisconsin–Madison.

During the summer of 1999, he was a visiting Ph.D. student at the DSPS R&D Texas Instruments Inc., Dallas, TX, working on antenna array diversity for wide-band CDMA. His research interests include wireless communications, information theory, and signal processing for communications.

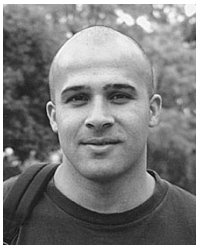

Akbar M. Sayeed (S'87–M'97) received the B.S. degree from the University of Wisconsin–Madison in 1991, and the M.S. and Ph.D. degrees in 1993 and 1996, respectively, from the University of Illinois at Urbana–Champaign, all in electrical and computer engineering.

While at the University of Illinois, he was a Research Assistant in the Coordinated Science Laboratory and was also the Schlumberger Fellow in Signal Processing from 1992 to 1995. During 1996–1997, he was a Postdoctoral Fellow at Rice University, Houston, TX. Since August 1997, he has been with the University of Wisconsin–Madison, where he is currently an Assistant Professor in Electrical and Computer Engineering. His research interests include wireless communications, statistical signal processing, time frequency and wavelet analysis.

Dr. Sayeed received the NSF CAREER Award in 1999. He is currently serving as an Associate Editor for the IEEE SIGNAL PROCESSING LETTERS.

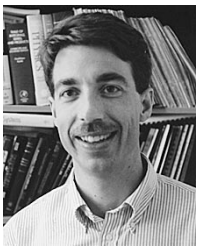

Barry D. Van Veen (S'81–M'83–SM'97) was born in Green Bay, WI. He received the B.S. degree from Michigan Technological University in 1983 and the Ph.D. degree from the University of Colorado in 1986, both in electrical engineering. He was an ONR Fellow while working toward the Ph.D. degree.

In the spring of 1987, he was with the Department of Electrical and Computer Engineering at the University of Colorado–Boulder. Since August of 1987, he has been with the Department of Electrical and Computer Engineering at the University of Wisconsin–Madison and currently holds the rank of Professor. He co-authored the book "Signals and Systems" (New York: Wiley, 1999) with Simon Haykin. His research interests include signal processing for sensor arrays, nonlinear systems, adaptive filtering, wireless communications, and biomedical applications of signal processing.

Dr. Van Veen was a recipient of a 1989 Presidential Young Investigator Award from the National Science Foundation and a 1990 IEEE Signal Processing Society Paper Award. He served as an Associate Editor for the IEEE Transactions on Signal Processing and on the IEEE Signal Processing Society's Technical Committee on Statistical Signal and Array Processing from 1991 to 1997. He received the Holdridge Teaching Excellence Award from the ECE Department at the University of Wisconsin in 1997.